

Traversing the Continuous Spectrum of Image Retrieval with Deep Dynamic Models

Ziad Al-Halah¹

ziadhlh@gmail.com

¹Karlsruhe Institute of Technology

Andreas M. Lehrmann

andreas.lehrmann@gmail.com

²Vector Institute

Leonid Sigal^{2,3}

lsigal@cs.ubc.ca

³University of British Columbia

Abstract

We introduce the first work to tackle the image retrieval problem as a continuous operation. While the proposed approaches in the literature can be roughly categorized into two main groups: category- and instance-based retrieval, in this work we show that the retrieval task is much richer and more complex. Image similarity goes beyond this discrete vantage point and spans a continuous spectrum among the classical operating points of category and instance similarity. However, current retrieval models are static and incapable of exploring this rich structure of the retrieval space since they are trained and evaluated with a single operating point as a target objective. Hence, we introduce a novel retrieval model that for a given query is capable of producing a dynamic embedding that can target an arbitrary point along the continuous retrieval spectrum. Our model disentangles the visual signal of a query image into its basic components of categorical and attribute information. Furthermore, using a continuous control parameter our model learns to reconstruct a dynamic embedding of the query by mixing these components with different proportions to target a specific point along the retrieval simplex. We demonstrate our idea in a comprehensive evaluation of the proposed model and highlight the advantages of our approach against a set of well-established discrete retrieval models.

1. Introduction

Image retrieval is a primary task in computer vision and a vital precursor for a wide range of topics in visual search. The core element of each retrieval algorithm is a procedure that queries an image database and returns a ranked list of images that are close to the query image. The ranking is defined with respect to a retrieval objective and a corresponding distance metric. The retrieval objective can be any underlying property of an image, such as its categories (e.g., car, table, dog) [11, 18] or its visual attributes (e.g., metallic, hairy, soft) [8, 42]. This objective is expressed during training with a suitable criterion (e.g., a cross entropy loss for categories) to encode the relevant information

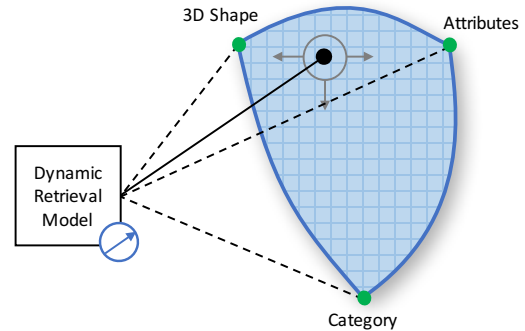


Figure 1: Unlike classical *discrete* retrieval models operating at a single point like category- or attribute-based retrieval (green points), we propose to consider the full *continuous* spectrum of the retrieval simplex (blue surface). Our model dynamically constructs a query embedding to target an arbitrary operating point on the simplex (black point).

in a learned, low dimensional feature space (i.e., the embedding space) [19, 35]. The distance metric is typically an Euclidean distance or a learned metric that captures the pairwise similarity in the respective embedding space.

While this classical approach works well in practice, it is also static and inflexible. Once the model is trained, we can only retrieve images based on the single retrieval objective chosen at training time, e.g., images with similar attributes or with similar categories. However, the space of image-metadata is rich. Each new type of hand-annotated or machine-inferred data constitutes an independent axis of interest that retrieval models should account for (e.g., objects, captions, and other types of structured data related to the composition of a scene). A simple way to incorporate such diverse objectives during the retrieval process is to learn a joint embedding with a hyper approach [26]. This is not desirable for the following reasons: (1) It reduces the amount of available training data to the point where standard training techniques become infeasible. (2) The semantic axes of interest are often orthogonal (e.g., a cat can be white, but not all cats are white and not all white objects are cats), hence augmenting the label space through such a cou-

pling is neither flexible nor scalable. (3) The contributions of the individual objectives are fixed and unweighted.

Instead, we propose a novel retrieval concept that accounts for retrieving images based on a convex combination of multiple objectives in a continuous manner (Fig. 1). Hence, any valid weighting on this simplex of retrieval objectives can be chosen at *test-time*. We refer to a specific point on this simplex as the *simplicial retrieval operating point* (SROP). In this work, we explore a setting with two retrieval objectives: categories and attributes. We propose a novel approach that allows targeting a specific SROP at test time. The resulting model can be viewed as a continuous slider that can retrieve images based on the query image’s category, its attributes or any other SROP between those two extremes (e.g., an equal weighting between both). The representation disentangling between categories and attributes is achieved through parallel memory networks learning corresponding prototypes. In particular, we assign a memory for generalization, where we capture categorical prototypes, and another one for specification, where we capture attribute-based prototypes. Both memories are learned end-to-end based on gated backpropagation of gradients from custom losses, one for each respective objective. Crucially, both the gates and the losses are SROP-weighted. At test-time, our model can *dynamically* predict the suitable embedding of an image for a targeted SROP by retrieving and mixing the relevant prototypes learned in both memories.

Contributions We make the following contributions in this work: (1) we introduce the first work to address image retrieval as a continuous task, namely spanning the continuous spectrum between different operating points; (2) we propose a novel *continuous* retrieval module allowing test-time selection of a simplicial retrieval operating point in a smooth and dynamic fashion; (3) we introduce and validate novel optimization techniques that are necessary for efficient and effective learning of the retrieval modules; (4) we evaluate the advantages of our approach against the classical *discrete* deep retrieval models and demonstrate its effectiveness in a real world application of visual fashion retrieval.

2. Related Work

The bulk of image retrieval research can be split into two main groups: instance- and category-based retrieval. In *instance-based* retrieval we want to retrieve images of the exact same object instance presented in a query (potentially in a different pose or from a different viewing angle). Early work in this direction focused on matching low-level descriptors [21, 29, 36, 43], learning a suitable similarity metric [20, 27], or compact representation [6, 19, 35]. More recently, deep neural networks became predominant in the retrieval literature. CNNs, in particular, were used as off-the-shelf image encoders in many modern instance retrieval models [2, 3, 4, 12, 30, 33, 34, 37, 39, 40, 46]. Moreover,

siamese [32] and triplet networks [13, 16, 48, 53] demonstrated impressive performance as they provide an end-to-end framework for both embedding and metric learning.

Category-based retrieval methods are on the other end of the retrieval spectrum. Here, the models target the semantic content of the query image rather than the specific instance. For example, given a query image of a house on the river bank, we are interested in retrieving images with similar semantic configuration (i.e., *house+river*) rather than images of the exact *blue* house with *red* door in the query. This type of model learns a mapping between visual representations and semantic content, which can be captured by image tags [10, 11, 18, 38], word vector embeddings [9, 31], image captions [14], or semantic attributes [8, 42, 17]. Most recently, hyper-models [25, 26, 47] are proposed to learn an image embedding by jointly optimizing for multiple criteria like category and attribute classification. However, these models operate at a fixed mixture point of the two retrieval spaces and not dynamically in between.

Differently, this work is the first to phrase the retrieval task as a continuous operation. Moreover, we propose a novel model that not only can operate at the two extremes of the retrieval spectrum but is also capable of dynamically traversing the simplex in between, generating intermediate retrieval rankings. Hence, it effectively provides an infinite set of retrieval models in one and can target the desired operating point at test-time using a control parameter.

Our model is based on memory networks [44, 49] which have proven useful in many applications, including text-based [5, 23, 28, 44, 49] and vision-based [45, 50, 51] question answering and visual dialogs [7, 41]. Here, we present a novel type of memory network architecture that learns and stores visual concept prototypes. We propose two types of memories to distinguish between categorical- and instance-based information. Moreover, we provide key insights on how to improve learning of these concepts in memory using a novel dropout-based optimization approach.

3. Dynamic Retrieval Along a Simplex

We propose an image retrieval approach that operates dynamically along the retrieval simplex. We achieve this with a deep model that distills the visual signal from a query image into its basic components (in this case category- and attribute-relevant components) and then blends them to target an arbitrary retrieving operation point. Specifically, using a novel memory network architecture (Fig. 2), our model learns various visual prototypes present in the data and stores them in the memory. The prototypes can be understood as non-linear sets of basis vectors separately encoding category- and attribute- information. Given a query image and a control parameter, our model learns to retrieve the relevant prototypes from memory and combines them in appropriate proportions. Thus, it constructs a custom em-

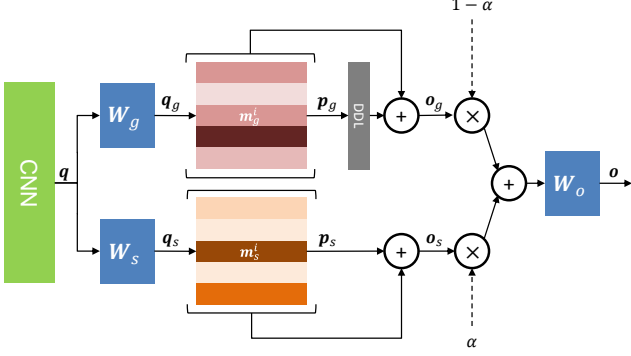


Figure 2: **Dynamic Retrieval Network.** Two parallel memory modules encode category and attribute prototypes that are fused based on a test-time selection of mixing coefficients on a simplex.

bedding of the query to target a specific operating point on the retrieval simplex (SROP).

Overview Given an image x encoded with $\mathbf{q} = f(x)$ (e.g., a CNN), our proposed dynamic retrieval network (DRN) has the following main components: 1) A *query module*, which projects the generic query embedding \mathbf{q} into category- (\mathbf{q}_g) and attribute-specific (\mathbf{q}_s) representations to address our parallel memory module; 2) A *memory module*, which learns visual concept prototypes in a generalization (\mathbf{M}_g) and a specification (\mathbf{M}_s) memory. Both \mathbf{q}_\bullet and \mathbf{M}_\bullet are combined to form a category (\mathbf{o}_g) and attribute (\mathbf{o}_s) representation for the query image. Finally, 3) An *output module*, which mixes the constructed representations with different proportions given a *specificity* control parameter α . The query embedding derived by the output module is then compared (e.g., using Euclidean distance) to similarly computed embeddings of each image in the dataset to arrive at the ranked list of retrieved images. Next, we provide a detailed description of our DRN and its components.

3.1. Query module

Given an image x encoded with a deep network, $\mathbf{q} = f(x)$, we query each memory module using \mathbf{q}_s and \mathbf{q}_g . These two queries are learned using two different projection layers $f_s(\cdot)$ and $f_g(\cdot)$ to adapt to the different representations in \mathbf{M}_g and \mathbf{M}_s :

$$\begin{aligned} \mathbf{q}_g &= f_g(x) = \mathbf{W}_g f(x) + b_g, \\ \mathbf{q}_s &= f_s(x) = \mathbf{W}_s f(x) + b_s, \end{aligned} \quad (1)$$

where \mathbf{W}_\bullet and b_\bullet are the weights and bias for each layer.

3.2. Memory Modules

To operate dynamically at an arbitrary SROP, we need to control the information embedded in the query representation. Hence, we propose to factorize the representation of an input x in terms of a category- and attribute-based representation. While the category-based representation captures the shared information between x and all samples of the same category as x , the attribute-based representation

captures the information that distinguishes x from the rest (i.e., its visual attributes). By separating the two signals, we control how to mix these two representations to construct a new embedding of x that targets the desired SROP on the retrieval simplex. Hence, our memory module is made up of two parallel units: a) The *generalization memory* (\mathbf{M}_g), that learns category-based prototypes; and b) The *specification memory* (\mathbf{M}_s), that learns attribute-based prototypes.

Generalization Memory Here, we would like to learn concept prototypes that capture information shared among all samples of the same category. Based on the intuitive assumption that samples usually belong to a single (or a few) base categories, we can use a softmax layer to attend to the memory cells of \mathbf{M}_g . Given the sparse properties of a softmax layer, this allows us to learn a discriminative category-based representations and attend to the most suitable one to construct the input embedding. That is, given a query \mathbf{q}_g , the category-based embedding of \mathbf{q}_g is constructed as:

$$\begin{aligned} p_g^i &= \text{softmax}(\mathbf{q}_g^\top \mathbf{m}_g^i), \\ \mathbf{o}_g &= \sum_i^{N_g} p_g^i \mathbf{m}_g^i, \end{aligned} \quad (2)$$

where p_g^i is the attention over memory cell \mathbf{m}_g^i , N_g is the total number of generalization memory cells, and \mathbf{o}_g is the output of the generalization memory module \mathbf{M}_g .

Dropout Decay Layer (DDL) While the sparsity of the softmax is beneficial to learn discriminative prototypes, it may result in stagnation during the optimization process since the backpropagated error signals get channeled to a few memory cells. To counter these optimization difficulties caused by the softmax layer, we propose a *dropout decay layer* (DDL) over the attentions p_g . The DDL is a dropout layer with an initial dropout probability p_d and a decay factor γ_d . Starting with an initially high dropout rate p_d , the DDL pushes our model to activate and initialize many cells in \mathbf{M}_g rather than relying on just a few. As the training progresses, the dropout probability gradually gets dampened by γ_d , enabling the model to learn a more discriminative representation in \mathbf{M}_g .

Specification Memory While each sample typically belongs to a single base category, it usually exhibits a set of multiple visual attributes that are instance specific and distinguish this instance from others within the same category. Hence, we use a sigmoid layer to attend to the memory cells of \mathbf{M}_s , which allows us to select and compose multiple attributes. Given a query \mathbf{q}_s , we construct the attribute-based representation \mathbf{o}_s as follows:

$$\begin{aligned} p_s^j &= \text{sigmoid}(\mathbf{q}_s^\top \mathbf{m}_s^j), \\ \mathbf{o}_s &= \frac{1}{\sum_j p_s^j} \sum_j^{N_s} p_s^j \mathbf{m}_s^j, \end{aligned} \quad (3)$$

where p_s^j is the attention over memory cell \mathbf{m}_s^j , N_s is the number of cells in \mathbf{M}_s , and \mathbf{o}_s is the output of the specification memory module. Unlike softmax, the sigmoid layer does not produce a sparse attention over \mathbf{M}_s and hence we do not need a special activation mechanism as in \mathbf{M}_g .

3.3. Output Module

Given the output representation of the two memory modules, we construct the representation of input sample x as a weighted linear combination of \mathbf{o}_s and \mathbf{o}_g :

$$\mathbf{o} = f_o(\mathbf{o}_s, \mathbf{o}_g) = \mathbf{W}_o(\alpha \cdot \mathbf{o}_s + (1 - \alpha) \cdot \mathbf{o}_g) + b_o, \quad (4)$$

where $f_o(\cdot)$ is an embedding of the linear combination of the memory modules' outputs. The specificity control $\alpha \in [0, 1]$ weights the contribution of each memory module in the final representation of x . As α approaches zero, the category-based information of x is emphasized in \mathbf{o} . By increasing α , we incorporate more instance-specific information (with attributes as proxy) from x into \mathbf{o} .

3.4. Dynamic Learning Objective

To learn the representations in the memory cells of \mathbf{M}_g and \mathbf{M}_s , we need a learning objective that can distill the error signal dynamically into category- and attribute-based signals with proportions similar to the targeted SROP of the constructed embedding. We achieve this using multitask learning, *i.e.*, we jointly optimize for two criteria to capture both signals. Additionally, both criteria are weighted by the specificity parameter α that controls the contributions of the backpropagated error signals to the memory modules. We consider two options:

1) Classification-based DRN (DRN-C) This model is optimized jointly for category and attribute classification:

$$\mathcal{L}(x) = (1 - \alpha)\mathcal{L}_{cls}(x) + \alpha\mathcal{L}_{att}(x) + \beta\mathcal{L}_{reg}(\theta) \quad (5)$$

where \mathcal{L}_{cls} and \mathcal{L}_{att} are cross entropy losses for the categories and attributes, respectively, and $\mathcal{L}_{reg} = \|\theta\|_2^2$ is a regularization loss over the model parameters θ .

2) Similarity-based DRN (DRN-S) This model optimizes jointly for category classification and pairwise instance similarity:

$$\mathcal{L}(x_1, x_2) = (1 - \alpha)(\mathcal{L}_{cls}(x_1) + \mathcal{L}_{cls}(x_2)) + \alpha\mathcal{L}_{sim}(x_1, x_2) + \beta\mathcal{L}_{reg}(\theta), \quad (6)$$

where \mathcal{L}_{cls} and \mathcal{L}_{reg} are defined as above and \mathcal{L}_{sim} is a margin-based contrastive loss [15].

DRN-C and DRN-S have different characteristics: Since DRN-C is optimized with cross entropy losses, we expect a strong discriminative error signal from object and attribute losses, which will help in learning more discriminative prototypes. On the other hand, DRN-S leverages a contrastive

loss that captures the generic pairwise similarity of samples in the attribute embedding space. Experimentally, we find that this lends itself well to cases where it is desirable to maintain the category as α changes. Intuitively, DRN-S can be considered to be more generic than DRN-C, since arbitrary similarity metrics can be used in this formulation (*e.g.*, caption similarity) to define the extrema of the retrieval simplex and, consequently, the SROPs that we wish to traverse.

Sampling α For each training image x , we sample α randomly from $[0, 1]$ using a uniform distribution. Note that α not only controls the mixing of category- and attribute-based prototypes, but also controls the error signal coming from the category- and attribute-based losses. α acts as a gating layer which controls the flow of information to each memory module and allows us to distill the backpropagated error signal during training. At test time, we can select α freely to control the SROP, which can be anywhere between pure category-prototypes and pure attribute-based ones.

4. Evaluation

Our experiments evaluate our model's ability to operate along the retrieval simplex. We first conduct a thorough evaluation of the modules proposed in Sec. 3 by validating our design choices and their impact on the performance and the learned concept prototypes (Sec. 4.1). Next, we evaluate both DRN-C and DRN-S in the proposed retrieval task and highlight their distinct properties. A comparison to popular baselines demonstrates the advantages of our approach (Sec. 4.2). We conclude with the analysis of our model in a fashion retrieval application (Sec. 4.3).

MNIST Attributes We evaluate our model on the MNIST Attribute dataset, which is driven from the MNIST [24] and MNIST Dialog [41] datasets. In particular, each digit image of the 10 classes is augmented with 12 binary visual attributes: 5 foreground colors of the digit, 5 background colors, and 2 style-related attributes (*stroke*, *flat*). In total, we have 20,000 images for training, 5,000 for validation, and 5,000 for testing (see Fig. 8).

Model Architecture In order to guarantee a fair comparison, we use the same core CNN (green box in Fig. 2) in all our experiments: the first 2 layers consist of convolutions with kernel size 5 and 20/50 feature maps, respectively. Both layers are followed by a max-pooling layer with stride 2. The core CNN ends with 2 fully-connected layers with ReLU activations of size 500. We combine this core CNN with the modules illustrated in Fig. 2 to obtain our full dynamic model and with various classifiers for our baseline comparisons. We train all models using Adam [22] with an initial learning rate of 10^{-4} .

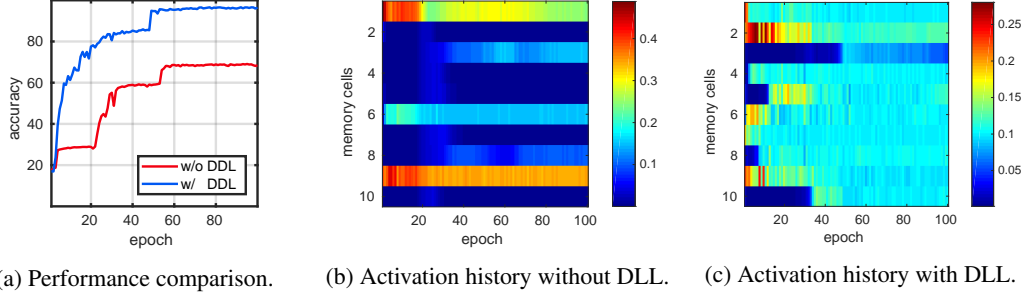


Figure 3: **Analysis of the dropout decay layer (DDL).** (a) DDL leads to significant improvements in both performance and convergence rate. (b) Without DDL, the model tends to rely on a few learned prototypes for extended periods of time, resulting in performance stagnation. (c) With DDL, the model is incentivized to activate additional memory cells early in the training process.

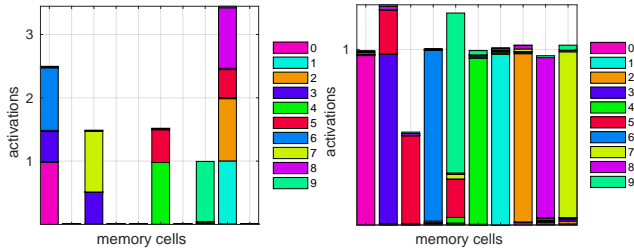


Figure 4: **Prototypes learned in memory.** Visualization of cell activation (left) without dropout decay layer and (right) with dropout decay layer. Colors indicate utilization of cells by a particular digit.

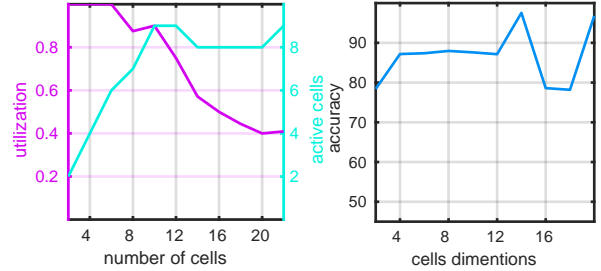


Figure 5: **Effect of number and dimensionality of cells in M_g .** (left) Memory utilization across number of cells. (right) Model performance across cell dimensionality.

4.1. Learning Visual Concept Prototypes

We start by analyzing the properties of our memory modules. Hence, we train a CNN augmented with our generalization memory M_g and followed by a softmax layer for category classification and use a cross-entropy loss. We set the number of cells in M_g to $N = 10$ and the initial dropout probability to $p_d = 0.9$, with a decay of $\gamma_d = 10^{-5}$.

Dropout Decay Layer (DDL) Fig. 3a shows the performance of our model with and without the proposed DDL. The model without DDL suffers from long periods of stagnation in performance (red curve). To better understand this phenomenon, we track, during learning, the activation history of the memory cells across the entire training dataset: examining Fig. 3b, we notice that overcoming these stages of stagnation actually corresponds to the activation of a new memory cell, *i.e.*, a new category prototype. DDL significantly improves the performance of the model by pushing it to activate multiple memory cells early in the training process rather than relying on a few initial prototypes (Fig. 3c). Moreover, the early epochs of training are now characterized by high activations of multiple cells, which gradually get dampened in the later stages. In summary, DDL not only counteracts the stagnation in training but also results in faster convergence and better overall performance.

Memory Semantics To gauge what the model actually captures in memory, we validate it on test data by accu-

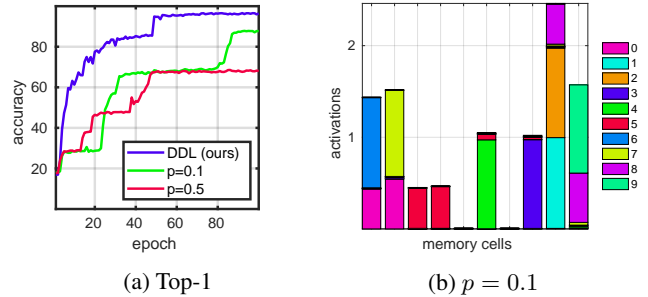


Figure 6: **Comparison to constant dropout.** (a) DDL performs significantly better than a network with constant dropout. (b) Constant dropout with $p = 0.1$ leads to mixing artifacts similar to a network without DDL (cf. Fig. 4(left)).

mulating a histogram of each cell’s activations over the categories: Fig. 4(right) shows the average activations per category for each cell. We see that our model learns a clean prototype in each cell for each of the categories. In comparison to a model without DDL (Fig. 4(left)), the learned representations in memory are substantially more discriminative.

Constant Dropout Interestingly, DDL is also more effective than standard dropout with fixed values $p = 0.1$ and $p = 0.5$ (*i.e.* without decay): in addition to improved performance (Fig. 6a), we see in Fig. 6b that such a fixed dropout probability leads to learning mixed category prototypes in

the memory cells. For some categories, their prototypes are split across multiple cells, while other cells capture a generic prototype that represents multiple categories. This is expected: due to the constant dropout during training, multiple cells are forced to capture similar category prototypes in order to cover the information loss encountered from dropping out some of the cells.

Memory Configuration Our memory module is parametrized by the number of cells N and their dimensionality d . We analyze the impact of these hyperparameters on memory utilization and model performance in the following experiments:

- *Number of Cells:* We vary the number of cells in the memory and check how many of them are utilized. We measure utilization as the percentage of cells activated for at least 5% of the samples. Fig. 5(left) shows that utilization steadily drops beyond 10 cells while the number of active cell remains stable at 8 or 9, which is close to the number of categories in the dataset. We conclude that our model learns a sparse representation of the categories and uses the memory in a way that is consistent with the visual concepts present in the data. In other words, the model is not sensitive to this parameter and can effectively choose an appropriate number of needed active cells.

- *Dimensionality:* We analyze the impact of cell dimensionality on the final performance of the model. We set our memory module to $N = 10$ cells and vary the dimensionality d . Fig. 5(right) shows the change in classification accuracy along d . Our model exhibits good robustness with regard to memory capacity and reaches 89% accuracy even with a low-dimensional representation.

While we analyzed the performance of the generalization memory, the analysis of specification memory looks similar, despite the denser activation patterns caused by the sigmoid (vs. softmax) attention for cell referencing.

4.2. From Category- to Attribute-based Retrieval

So far, we have evaluated our memory module and the impact of its configuration on utilization and accuracy. Next, we examine the performance and properties of our dynamic models along the retrieval simplex.

We train our full DRN models with both generalization and specification memories using the dynamic learning objectives. The CNN encoder in this experiment is identical to the one we used in Sec. 4.1. However, in this experiment, we train our model for 2 objectives that capture category- and attribute-based information, as explained in Sec. 3.4. While DRN-C is trained for a joint objective of category and attribute classification, the DRN-S model is trained for category classification and pairwise similarity, *i.e.*, a sample pair is deemed similar if they share the same attributes. During training, we sample α uniformly in the range $[0, 1]$

to enable the models to learn how to mix the visual concept prototypes at different operating points.

We measure the performance of category-based retrieval using C-TopK accuracy, which measures the percentage of the top K similar samples with matching category label to the query q . We measure the attribute-based performance using the A-TopK accuracy, which measures the percentage of matching attributes in the top K similar samples to q . At test time, we randomly sample 10 queries from each category and rank the rest of the test data with respect to the query using Euclidean distance as the similarity metric. The samples are embedded by the dynamic output of our DRN while gradually changing α from 0 to 1 to target the different SROPs.

Fig. 7 shows the retrieval performance of the proposed DRN-C and DRN-S. As α goes from 0 to 1, category-based accuracy (C-Top) decreases and attribute-based accuracy (A-Top) increases in the classification-based model DRN-C, as expected (Fig. 7a). The similarity-based model DRN-S, on the other hand, shows a stable, high performance for the category-based retrieval with varying α and shares similar properties of the attribute-based performance with the previous model, albeit with larger dynamic range (Fig. 7b). In summary, DRN-C helps us to cross the category boundary of the query to retrieve instances with similar attributes but from different categories. DRN-S model traverses the manifold within the category boundaries and retrieves instances from the same category as the query with controllable attribute similarity. These conclusions are reinforced by our qualitative results, which we discuss next.

Qualitative Results Fig. 8 shows qualitative results of both models: the first row (Q) is the query and each column displays the top K retrieved instances as α goes from 0 (left-most column) to 1 (right-most column). In case of the DRN-C model (Fig. 8a), we see that the left-most column contains samples with the correct category of the query but with diverse attributes. As we move toward $\alpha = 1$, we retrieve instances with more matching attributes but also from increasingly more diverse categories. With the DRN-S model (Fig. 8b), we can traverse from $\alpha = 0$ to $\alpha = 1$ while keeping the categorical information of the query, with increasing similarity of instance-specific information. We note that both of these behaviors may be desirable, depending on the application. For example, for a generic image retrieval, control over *specificity* of results may be desired, as is achieved with the DRN-S model; however, for exploring fashion apparel (Sec. 4.3) with a given style, the DRN-C model may be more appropriate.

Comparison to Baselines We compare our approach to 4 well-established *discrete* retrieval models:

- Siamese Network (SiamNet [32]): a siamese model that captures the pairwise similarity of samples.
- Attribute Network (AttNet [8, 17]): a deep model trained

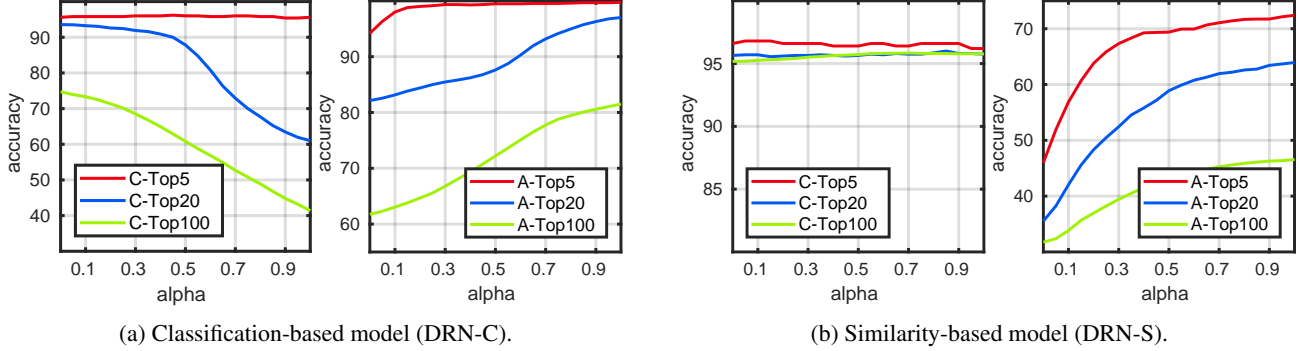


Figure 7: **Traversing the retrieval simplex.** We show the performance of our (a) DRN-C and (b) DRN-S as α increases from 0 to 1.

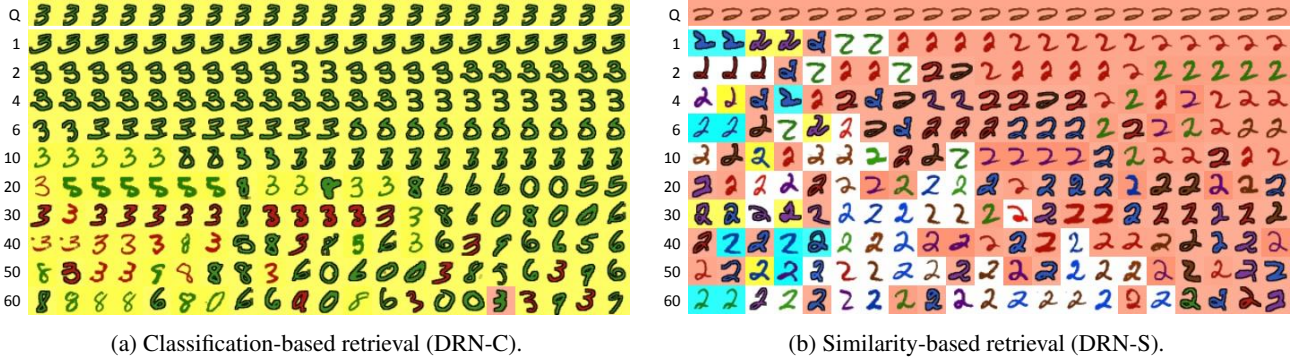


Figure 8: **Qualitative results.** The query (Q) is shown in the first row, the results with indicated rank K in the subsequent rows. Each column corresponds to the result for a particular value of α , from 0 (first column; focused on classification) to 1 (last column; focused on attributes). (a) The DRN-C model retrieves the correct class for $\alpha = 0$ and smoothly changes to the correct attributes for $\alpha = 1$ (neglecting class membership). (b) The DRN-S model keeps the correct class membership while increases attribute similarity as α approaches 1.

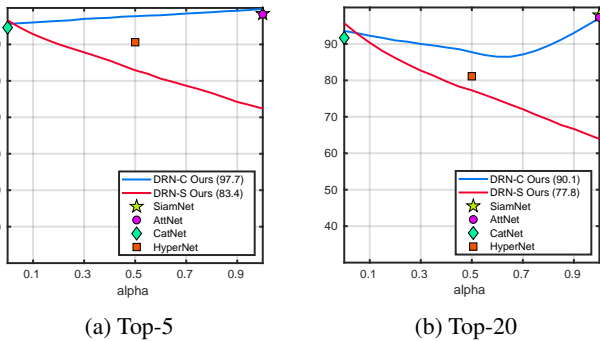


Figure 9: **Performance comparison to baselines.** We show (a) top-5 and (b) top-20 retrieval accuracy of 4 baseline discrete models (marks) and the two proposed dynamic models (solid lines) as α smoothly changes from 0 to 1. The proposed models are superior to the baselines and stable across the entire range of α , as indicated by the area under the curve shown in parenthesis.

for attribute classification.

- Categorization Network (CatNet [4, 12]): a deep model trained for category classification.
- Hyper Network (HyperNet [26]): a deep model trained

for the joint objective of predicting both categories and attributes with equal weighting.

We implement these models and adopt them to our problem and dataset. All baseline models use the same core CNN structure as our own models (see Sec. 4). We represent each image using the output of the last hidden layer of the respective model. The retrieval is conducted as in the previous experiment, *i.e.*, the query image is compared against all samples in the dataset and ranked using Euclidean distance.

To the best of our knowledge, our model is the first one allowing the retrieval at different operating points of the retrieval simplex. Since there are no standard performance measures for this task, we introduce a new measure of performance along the continuous retrieval simplex, namely the α -weighted average of category and attribute accuracy for the top- K retrieved samples:

$$\text{Top}_K = \alpha \text{Top}_K^A + (1 - \alpha) \text{Top}_K^C. \quad (7)$$

Fig. 9 shows the performance of our models compared to the classical retrieval models. Note that the discrete models generate a *single* static ranking and excels at a specific point on the retrieval simplex. These optimal SROPs of each of

these models are highlighted with a marker. We see that SiamNet and AttNet operate at $\alpha = 1$, because their embeddings are optimized with the objective of attribute similarity. CatNet, on the other hand, operates at $\alpha = 0$, since it is optimized with the objective of category classification. The HyperNet model operates at $\alpha = 0.5$, in accordance with the optimization of both category and attribute objectives. Our DRN-S model is the best-performing model at $\alpha = 0$ but declines lower than HyperNet as α goes to 1. We believe this is because the DRN-S tries to incorporate attribute information in addition to categorical information, which is substantially harder than a trade-off between both objectives. Despite lower performance at certain SROPs, DRN-S does exhibit useful behavior in practice. Finally, our DRN-C model shows the best overall performance along the retrieval simplex, exhibiting consistently good performance as it traverses between the two extremes of $\alpha = 0$ and $\alpha = 1$ and even outperforms the discrete models at their optimal SROPs.

4.3. Traversing Visual Fashion Space

We conclude with an application of our dynamic model to the real-world task of fashion exploration, where it allows the interactive traversal between the category and visual style (*i.e.* attributes) of a query fashion item.

We test our model on two large-scale fashion datasets: **1)** The UT-Zappos50K dataset [52] which contains around 50,000 images of footwear items. The items fall into 4 main categories (Sandals, Boots, Shoes, and Slippers). We select 20 out of the most frequent tags provided by the vendors as the attribute labels for the images. These attributes describe properties such as gender, closure-type, heel-height and toe-style. **2)** The Shopping100K [1] which has around 100,000 images of clothes from 16 categories (*e.g.* Shirts, Coats and Dresses). Additionally, all images are labeled with 135 semantic attributes that describe visual properties like collar-type, sleeve-length, fabric and color. We split each dataset with a ratio of 1 to 9 for testing and training. We train our DRN-C and 3 discrete baselines that share the same backbone architecture with our model, similar to the setup in our previous experiments.

Fig. 10 shows the performance of our model compared to the baselines in terms of top-20 accuracy. As before, we see that overall our DRN-C model outperforms its competitors with a significant margin ($\approx 4\%$). Comparing Fig. 10 to Fig. 9, it is also evident that attribute retrieval on both datasets is substantially more complex than on MNIST Attributes. Even AttNet, which should operate optimally at $\alpha = 1$, shows a performance closer to HyperNet or worse. Upon further inspection, we notice that some of the attributes have strong correlation with category labels. For instance, attributes related to heel-heights or toe-styles appear almost exclusively with women’s shoes, rendering learning

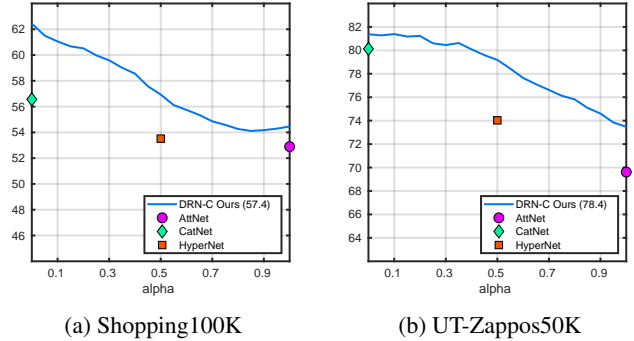


Figure 10: **Performance comparison to baselines on fashion retrieval.** We show top-20 retrieval accuracy on (a) Shopping100K [1] and (b) UT-Zappos50K [52] of 3 discrete retrieval models (marks) and our proposed model DRN-C (solid line) as α smoothly changes from 0 to 1.

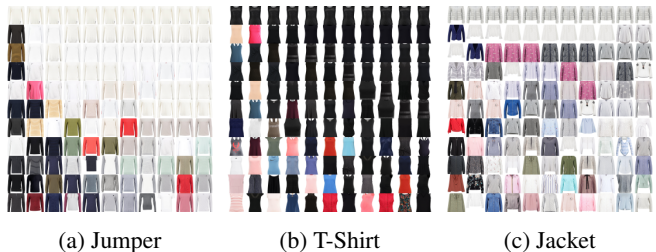


Figure 11: **Qualitative results on Shopping100K.** As the control parameter α goes from 0 (left) to 1 (right), the SROP for each query (1^{st} row) changes from pure category retrieval to style-based retrieval, *i.e.* attribute-based retrieval. Best viewed in color and with zoom-in.

an attribute representation that is disentangled from the associated categories challenging. Our model handles these cases well and performs significantly better than all competing methods at their optimal SROPs. Similar to Fig. 8, we show qualitative examples on Shopping100K in Fig. 11, illustrating our model’s ability to smoothly interpolate between categories and styles in fashion space.

5. Conclusion

We introduced the first work to address the retrieval task as a continuous operation traversing the retrieval simplex smoothly between different operating points (SROPs). We proposed a novel dynamic retrieval model DRN that can target the desired SROP along the simplex using a control parameter. Moreover, we presented key insights on how to optimize training and improve learning of such a model using the proposed dropout decay layer. We demonstrated the properties and differences between two dynamic learning schemes and highlighted the performance of our model against a set of established discrete deep retrieval models. Finally, we hope that our findings will be a stepping stone for further research in the direction of traversing the continuous spectrum of image retrieval.

References

- [1] K. E. Ak, A. A. Kassim, J. Hwee Lim, and J. Yew Tham. Learning attribute representations with localization for flexible fashion search. In *CVPR*, 2018. 8
- [2] H. Azizpour, A. Sharif Razavian, J. Sullivan, A. Maki, and S. Carlsson. From generic to specific deep representations for visual recognition. In *CVPR Workshops*, 2015. 2
- [3] A. Babenko and V. Lempitsky. Aggregating local deep features for image retrieval. In *ICCV*, 2015. 2
- [4] A. Babenko, A. Slesarev, A. Chigorin, and V. Lempitsky. Neural codes for image retrieval. In *ECCV*, 2014. 2, 7
- [5] A. Bordes, N. Usunier, S. Chopra, and J. Weston. Large-scale simple question answering with memory networks. *arXiv preprint arXiv:1506.02075*, 2015. 2
- [6] Y. Cao, M. Long, B. Liu, and J. Wang. Deep cauchy hashing for hamming space retrieval. In *CVPR*, June 2018. 2
- [7] A. Das, S. Kottur, K. Gupta, A. Singh, D. Yadav, J. M. Moura, D. Parikh, and D. Batra. Visual dialog. *arXiv preprint arXiv:1611.08669*, 2016. 2
- [8] X. Y. Felix, R. Ji, M.-H. Tsai, G. Ye, and S.-F. Chang. Weak attributes for large-scale image retrieval. In *CVPR*, 2012. 1, 2, 6
- [9] A. Frome, G. S. Corrado, J. Shlens, S. Bengio, J. Dean, M. Ranzato, and T. Mikolov. DeViSE: A Deep Visual-Semantic Embedding Model. In *NIPS*, 2013. 2
- [10] Y. Gong, Q. Ke, M. Isard, and S. Lazebnik. A multi-view embedding space for modeling internet images, tags, and their semantics. *IJCV*, 106(2):210–233, 2014. 2
- [11] Y. Gong, S. Lazebnik, A. Gordo, and F. Perronnin. Iterative quantization: A procrustean approach to learning binary codes for large-scale image retrieval. *T-PAMI*, 35(12):2916–2929, 2013. 1, 2
- [12] Y. Gong, L. Wang, R. Guo, and S. Lazebnik. Multi-scale orderless pooling of deep convolutional activation features. In *ECCV*, 2014. 2, 7
- [13] A. Gordo, J. Almazán, J. Revaud, and D. Larlus. Deep image retrieval: Learning global representations for image search. In *ECCV*, 2016. 2
- [14] A. Gordo and D. Larlus. Beyond instance-level image retrieval: Leveraging captions to learn a global visual representation for semantic retrieval. In *CVPR*, 2017. 2
- [15] R. Hadsell, S. Chopra, and Y. LeCun. Dimensionality reduction by learning an invariant mapping. In *CVPR*, 2006. 4
- [16] E. Hoffer and N. Ailon. Deep metric learning using triplet network. In *International Workshop on Similarity-Based Pattern Recognition*, 2015. 2
- [17] J. Huang, R. S. Feris, Q. Chen, and S. Yan. Cross-domain image retrieval with a dual attribute-aware ranking network. In *ICCV*, 2015. 2, 6
- [18] S. J. Hwang and K. Grauman. Learning the relative importance of objects from tagged images for retrieval and cross-modal search. *IJCV*, 100(2):134–153, 2012. 1, 2
- [19] H. Jégou and O. Chum. Negative evidences and co-occurrences in image retrieval: The benefit of pca and whitening. In *ECCV*, 2012. 1, 2
- [20] H. Jégou, M. Douze, and C. Schmid. Improving bag-of-features for large scale image search. *IJCV*, 87(3):316–336, 2010. 2
- [21] H. Jégou, M. Douze, C. Schmid, and P. Pérez. Aggregating local descriptors into a compact image representation. In *CVPR*, 2010. 2
- [22] D. P. Kingma and J. L. Ba. ADAM: A Method for Stochastic Optimization. In *ICLR*, 2015. 4
- [23] A. Kumar, O. Irsoy, P. Ondruska, M. Iyyer, J. Bradbury, I. Gulrajani, V. Zhong, R. Paulus, and R. Socher. Ask me anything: Dynamic memory networks for natural language processing. In *ICML*, 2016. 2
- [24] Y. LeCun, L. Bottou, Y. Bengio, and P. Haffner. Gradient-based learning applied to document recognition. *Proceedings of the IEEE*, 86(11):2278–2324, 1998. 4
- [25] C. Li, C. Deng, N. Li, W. Liu, X. Gao, and D. Tao. Self-supervised adversarial hashing networks for cross-modal retrieval. In *CVPR*, 2018. 2
- [26] H. Liu, R. Wang, S. Shan, and X. Chen. Learning multifunctional binary codes for both category and attribute oriented retrieval tasks. In *CVPR*, 2017. 1, 2, 7
- [27] A. Mikulik, M. Perdoch, O. Chum, and J. Matas. Learning vocabularies over a fine quantization. *International journal of computer vision*, 2013. 2
- [28] A. Miller, A. Fisch, J. Dodge, A.-H. Karimi, A. Bordes, and J. Weston. Key-value memory networks for directly reading documents. *arXiv preprint arXiv:1606.03126*, 2016. 2
- [29] D. Nister and H. Stewenius. Scalable recognition with a vocabulary tree. In *CVPR*, 2006. 2
- [30] H. Noh, A. Araujo, J. Sim, T. Weyand, and B. Han. Large-scale image retrieval with attentive deep local features. In *ICCV*, 2017. 2
- [31] M. Norouzi, T. Mikolov, S. Bengio, Y. Singer, J. Shlens, A. Frome, G. S. Corrado, and J. Dean. Zero-Shot Learning by Convex Combination of Semantic Embeddings. In *ICLR*, 2014. 2
- [32] H. Oh Song, Y. Xiang, S. Jegelka, and S. Savarese. Deep metric learning via lifted structured feature embedding. In *CVPR*, 2016. 2, 6
- [33] M. Paulin, M. Douze, Z. Harchaoui, J. Mairal, F. Perronnin, and C. Schmid. Local convolutional features with unsupervised training for image retrieval. In *ICCV*, 2015. 2
- [34] F. Perronnin and D. Larlus. Fisher vectors meet neural networks: A hybrid classification architecture. In *CVPR*, 2015. 2
- [35] F. Perronnin, Y. Liu, J. Sánchez, and H. Poirier. Large-scale image retrieval with compressed fisher vectors. In *CVPR*, 2010. 1, 2
- [36] J. Philbin, O. Chum, M. Isard, J. Sivic, and A. Zisserman. Object retrieval with large vocabularies and fast spatial matching. In *CVPR*, 2007. 2
- [37] F. Radenović, G. Tolias, and O. Chum. Cnn image retrieval learns from bow: Unsupervised fine-tuning with hard examples. In *ECCV*, 2016. 2
- [38] V. Ranjan, N. Rasiwasia, and C. V. Jawahar. Multi-label cross-modal retrieval. In *ICCV*, 2015. 2

- [39] A. S. Razavian, H. Azizpour, J. Sullivan, and S. Carlsson. Cnn features off-the-shelf: an astounding baseline for recognition. In *CVPR Workshops*, 2014. 2
- [40] A. S. Razavian, J. Sullivan, S. Carlsson, and A. Maki. Visual instance retrieval with deep convolutional networks. *ITE Transactions on Media Technology and Applications*, 4(3):251–258, 2016. 2
- [41] P. H. Seo, A. Lehrmann, B. Han, and L. Sigal. Visual reference resolution using attention memory for visual dialog. In *NIPS*, 2017. 2, 4
- [42] B. Siddiquie, R. S. Feris, and L. S. Davis. Image ranking and retrieval based on multi-attribute queries. In *CVPR*, 2011. 1, 2
- [43] J. Sivic and A. Zisserman. Video google: A text retrieval approach to object matching in videos. In *ICCV*, 2003. 2
- [44] S. Sukhbaatar, J. Weston, R. Fergus, et al. End-to-end memory networks. In *NIPS*, 2015. 2
- [45] M. Tapaswi, Y. Zhu, R. Stiefelhagen, A. Torralba, R. Urta-sun, and S. Fidler. Movieqa: Understanding stories in movies through question-answering. In *CVPR*, 2016. 2
- [46] G. Tolias, R. Sivic, and H. Jégou. Particular object retrieval with integral max-pooling of cnn activations. In *ICLR*, 2015. 2
- [47] A. Veit, S. J. Belongie, and T. Karaletsos. Conditional similarity networks. In *CVPR*, 2017. 2
- [48] J. Wang, Y. Song, T. Leung, C. Rosenberg, J. Wang, J. Philbin, B. Chen, and Y. Wu. Learning fine-grained image similarity with deep ranking. In *CVPR*, 2014. 2
- [49] J. Weston, S. Chopra, and A. Bordes. Memory networks. In *ICLR*, 2015. 2
- [50] C. Xiong, S. Merity, and R. Socher. Dynamic memory networks for visual and textual question answering. In *ICML*, 2016. 2
- [51] H. Xu and K. Saenko. Ask, attend and answer: Exploring question-guided spatial attention for visual question answering. In *ECCV*, 2016. 2
- [52] A. Yu and K. Grauman. Fine-grained visual comparisons with local learning. In *CVPR*, 2014. 8
- [53] T. Yu, J. Yuan, C. Fang, and H. Jin. Product quantization network for fast image retrieval. In *ECCV*, 2018. 2